


## RESEARCH ARTICLE | *Neural Circuits*

# LFP clustering in cortex reveals a taxonomy of Up states and near-millisecond, ordered phase-locking in cortical neurons

 **Catalin C. Mitelut,<sup>1,2,3,4</sup> Martin A. Spacek,<sup>4,5</sup> Allen W. Chan,<sup>6</sup> Tim H. Murphy,<sup>2,3</sup> and Nicholas V. Swindale<sup>4</sup>**

<sup>1</sup>Department of Statistics, Columbia University, New York, New York; <sup>2</sup>Department of Psychiatry, Kinsmen Laboratory of Neurological Research, University of British Columbia, Vancouver, British Columbia, Canada; <sup>3</sup>Djavad Mowafaghian Centre for Brain Health, University of British Columbia, Vancouver, British Columbia, Canada; <sup>4</sup>Department of Ophthalmology and Visual Sciences, University of British Columbia, Vancouver, British Columbia, Canada; <sup>5</sup>Department of Biology II, Division of Neurobiology, Ludwig-Maximilians-Universität München, Munich, Germany; and <sup>6</sup>Department of Psychiatry, University of Alberta, Edmonton, Alberta, Canada

Submitted 17 July 2019; accepted in final form 6 August 2019

**Mitelut CC, Spacek MA, Chan AW, Murphy TH, Swindale NV.** LFP clustering in cortex reveals a taxonomy of Up states and near-millisecond, ordered phase-locking in cortical neurons. *J Neurophysiol* 122: 1794–1809, 2019. First published August 21, 2019; doi:10.1152/jn.00456.2019.—During slow-wave sleep and anesthesia, mammalian cortex exhibits a synchronized state during which neurons shift from a largely nonfiring to a firing state, known as an Up-state transition. Up-state transitions may constitute the default activity pattern of the entire cortex (Neske GT. *Front Neural Circuits* 9: 88, 2016) and could be critical to understanding cortical function, yet the genesis of such transitions and their interaction with single neurons is not well understood. It was recently shown that neurons firing at rates  $>2$  Hz fire spikes in a stereotyped order during Up-state transitions (Luczak A, McNaughton BL, Harris KD. *Nat Rev Neurosci* 16: 745–755, 2015), yet it is still unknown if Up states are homogeneous and whether spiking order is present in neurons with rates  $<2$  Hz (the majority). Using extracellular recordings from anesthetized cats and mice and from naturally sleeping rats, we show for the first time that Up-state transitions can be classified into several types based on the shape of the local field potential (LFP) during each transition. Individual LFP events could be localized in time to within 1–4 ms, more than an order of magnitude less than in previous studies. The majority of recorded neurons synchronized their firing to within  $\pm 5$ –15 ms relative to each Up-state transition. Simultaneous electrophysiology and wide-field imaging in mouse confirmed that LFP event clusters are cortex-wide phenomena. Our findings show that Up states are of different types and point to the potential importance of temporal order and millisecond-scale signaling by cortical neurons.

**NEW & NOTEWORTHY** During cortical Up-state transitions in sleep and anesthesia, neurons undergo brief periods of increased firing in an order similar to that occurring in awake states. We show that these transitions can be classified into distinct types based on the shape of the local field potential. Transition times can be defined to  $<5$  ms. Most neurons synchronize their firing to within  $\pm 5$ –15 ms of the transitions and fire in a consistent order.

clustering; local field potential; single-neuron recording; spike order; Up states

## INTRODUCTION

An established finding of the past several decades is that the cortical neurons of mammals spike differentially depending on behavioral state. During awake and attending periods and during rapid eye movement (REM) sleep, neurons fire largely independently of each other in a desynchronized state (Harris and Thiele 2011). During slow-wave sleep and anesthesia, a synchronized state is present where individual neurons cycle, at rates of 0.2–0.9 Hz, between a depolarized (spiking) state and a hyperpolarized (nonspiking) state. These are known as Up and Down states, respectively (McCormick and Yuste 2006; Neske 2016; Sanchez-Vives and McCormick 2000; Sanchez-Vives et al. 2017; Steriade et al. 1993). Up and Down states are brain-wide phenomena that engage cortex, thalamus, hippocampus, striatum, and cerebellum (Neske 2016). They may facilitate flexible processing of information (Haider et al. 2006; McCormick et al. 2004; McCormick and Yuste 2006) and may mediate changes in functional connectivity during waking states (Neske 2016). They also may be involved in memory replay (Sirota et al. 2003; Sirota and Buzsáki 2005; Wilson et al. 1994). Although Up-state-like transitions can be evoked by sensory or thalamic activation (Amzica and Steriade 1998; Steriade 2001), these transitions also occur spontaneously (Amzica and Steriade 1995; Destexhe et al. 1999; Volgushev et al. 2006). In addition, it has been suggested that the cortical “machinery” engaged by spontaneous Up-state transitions may be the same as that used to represent stimuli during awake, sleep, or anesthetized states (Amzica and Steriade 1998). More recently, a number of studies have found that high-firing-rate ( $>2$  Hz) neurons in rat somatosensory and auditory cortex spike in a similar order during Up-state transition as well as during the first 100 ms following stimulus onset (Bermudez-Contreras et al. 2013; Luczak et al. 2007, 2009), and it has been hypothesized that spike firing order may

Address for reprint requests and other correspondence: N. V. Swindale, Research Group, 2550 Willow St., Vancouver, BC, Canada V5Z 3N9 (e-mail: swindale@mail.ubc.ca).

represent “information packets” that pass from lower to higher cortical areas (Luczak et al. 2015). It also has been suggested that slow oscillations and synchronized states might provide a “unifying paradigm for the study of cortical function” (Sanchez-Vives et al. 2017).

Thus the precise temporal relationship between Up-state transitions and single-neuron firing is important, and tracking temporal firing order for all cells (not just high-firing-rate cells) and with high temporal precision (previous studies revealed 25- to 150-ms-wide responses in neurons) in all cortical areas and multiple mammalian species could help reveal a coding strategy used by cortex. However, current approaches have limitations to defining Up-state transitions with high temporal precision and for many neurons. Intracellular recordings can be used to define Up-state transitions with high precision (Chauvette et al. 2010; Seamari et al. 2007) but are limited to only a few neurons at a time. Extracellular recordings can contain many simultaneously recorded neurons, but analysis of these has generally relied on the use of peaks in firing rate histograms (Luczak et al. 2007), which tend to exclude low-firing-rate neurons (over 80% of neurons in our work fire <2 Hz; see Table 3) and rely on a somewhat arbitrary definition of Up-state onset time.

In the current study we show that in cats, mice, and rats, Up-state onset times can be defined with <5-ms precision by using multichannel local field potential (LFP) signals enabling the accurate measure of latencies of simultaneously recorded single units. Previous studies have shown that single-channel LFP events correlate with Up-state transitions (Chauvette et al. 2010; Saleem et al. 2010), and more recent work in rat hippocampal slices (Reichinnek et al. 2010) and anesthetized macaque hippocampus (Ramirez-Villegas et al. 2015) has shown that LFP events can have stereotyped shapes. In this study we cluster multichannel LFP signals and show that grouping the clusters using the current source density (CSD) laminar profile reveals multiple Up-state classes in cat, mouse, and rat cortex. We also show that neurons can synchronize their firing to within  $\pm 5$ –15 ms of Up-state transitions. These findings across three species and individual recordings add to the evidence that cortical neurons are capable of firing with high temporal precision relative to each other. Our findings that Up-state transitions fall into unique classes and that single-neuron firing order during such transitions is preserved on timescales of milliseconds support and extend previous research showing that firing rate order on a millisecond timescale may be important in cortical communication.

## MATERIALS AND METHODS

### Experimental Design

**Cat electrophysiological recordings.** Experimental procedures are described in detail in previous work (Swindale and Spacek 2014) and were carried out in accordance with guidelines established by the Canadian Council on Animal Care and institutional protocols reviewed and approved by the Animal Care Committee of the University of British Columbia. Data analyzed in this work were obtained from 15 electrode penetration sites in five adult cats (*animals C1–C5*). The cats were anesthetized either with 0.5–1.5% isoflurane and 70% N<sub>2</sub>O + 30% O<sub>2</sub> (*C1, C2, C3*) or with continuously infused propofol (6–9 mg·kg<sup>-1</sup>·h<sup>-1</sup>) and fentanyl (4–6  $\mu$ g·kg<sup>-1</sup>·h<sup>-1</sup>) (*C4, C5*). Following craniotomy surgery, a high-density polytrode was inserted perpendicularly into the cortex until the upper recording sites were 100–200  $\mu$ m below the surface. Polytrodes were either two (*C2, C4,*

*C5*) or three column (*C1, C3*) with electrode site spacing of 50–75  $\mu$ m. Voltage signals were analog bandpass filtered between 0.5 and 6 kHz, sampled at a rate of 25 kHz, and digitized with 12-bit resolution (Blanche et al. 2005). A subset of 10 electrode sites was used to separately record the LFP. Signals from these were bandpass filtered between 0.5 and 200 Hz and fed in parallel to separate amplifiers. On the three-column electrodes, the channels were 130  $\mu$ m apart, with the exception of the bottom two channels, which were 65 (*C1*) or 97  $\mu$ m (*C3*) apart. On the two-column electrodes, the channels were 150 (*C2, C4*) or 195  $\mu$ m (*C5*) apart, with the lower two channels being 100 (*C2, C4*) or 195  $\mu$ m (*C5*) apart. Recording sites were in area 17, and receptive fields (not reported here) were typically within 10° of the area centralis. In addition to recordings of spontaneous activity, visual stimuli including moving bars, gratings, *m*-sequence stimuli and natural scene movies were presented on a CRT screen. Table 1 summarizes recording IDs, anesthetic methods, and recording durations for individual experiments in cats.

**Rat electrophysiological recordings.** Extracellular recordings in rats were obtained from a publicly available database (<https://crcns.org/data-sets/fcx/fcx-1/about-fcx-1>, accessed April 21, 2019) and are described in detail in previous work (Watson et al. 2016). Briefly, Long-Evans rats between 4 and 7 mo of age were implanted with multishank (8 channels per shank) chronic extracellular probes in cortex. Recordings were made over periods of a few to several hours while the animals were alone in their home cages, during periods of wakefulness or periods of non-REM or REM sleep. For the current study, because of the lower density of the probes used (8 staggered channels) relative to the cat and mouse recordings (which had between 54 and 64 vertically parallel channels) and the limited spatial resolution, a single session from each of two rats was randomly selected and processed to evaluate the presence of Up-state clusters and single-neuron responses.

**Mouse electrophysiological recordings.** Experimental protocols were established and carried out in accordance with guidelines established by the Canadian Council on Animal Care and institutional protocols reviewed and approved by the Animal Care Committee of the University of British Columbia. Data reported here were obtained from a total of four electrode tracks in four mice (*C57/BL6*) anesthetized with isoflurane (1.5–2%) for surgery and with subsequent

Table 1. Cat visual cortex: recording summary

Rec ID	Anesthetic	Track ID	Sync Rec Time*/ Total Rec Time, h	No. of LECs
<i>C1.1</i>	Iso/N <sub>2</sub> O	1	0.6/13.4†	2
<i>C1.2</i>	Iso/N <sub>2</sub> O	2	1.4/9.4†	2
<i>C2.1</i>	Iso/N <sub>2</sub> O	1	1.7/11.1†	3
<i>C2.2</i>	Iso/N <sub>2</sub> O	2	4.7/12.0†	1
<i>C3.1</i>	Iso/N <sub>2</sub> O	1	1.4/8.4	1
<i>C3.2</i>	Iso/N <sub>2</sub> O	2	4.2/8.3	3
<i>C3.3</i>	Iso/N <sub>2</sub> O	3	3.4/7.4	2
<i>C3.4</i>	Iso/N <sub>2</sub> O	4	3.0/5.3	1
<i>C4.1</i>	Prop/Fent	1	3.3/11.9	1
<i>C4.2</i>	Prop/Fent	2	0.5/11.5	2‡
<i>C4.3</i>	Prop/Fent	3	0.9/4.6	2
<i>C5.1</i>	Prop/Fent	1	2.5/2.9	3
<i>C5.2</i>	Prop/Fent	2	4.9/10.6	3
<i>C5.3</i>	Prop/Fent	3	3.1/8.5	4
<i>C5.4</i>	Prop/Fent	4	4.6/6.3†	4
Total		15		34

Values are synchronized recording (Sync Rec) time/total recording time and number of local field potential (LFP) event clusters (LECs) for 15 recordings in cats. Recordings are identified (Rec IDs) by animal (*C1–C5*) and then by track number in each animal. \*Sync Rec time was defined as periods with synchrony index >0.5 unless otherwise indicated. †Synchrony index = 0.3. ‡LECs had peak-to-peak amplitude and current source density (CSD) maxima below threshold and were excluded from CSD grouping and further analysis. Fent, fentanyl; Iso, isoflurane; N<sub>2</sub>O, nitrous oxide; Prop, propofol.

Table 2. *Mouse cortex: recording summary*

Rec ID	Anesthetic	Track ID	Area	Imaging	Sync Rec Time/ Total Rec Time, h	No. of LECs
MV1	Isoflurane	1	Visual	VSD	2.6/3.1	2
MV2	Isoflurane	1	Visual	VSD	2.2/2.2	1
MV3	Isoflurane	1	Visual	No	2.5/2.5	2
MV4	Isoflurane	1	Visual	GCaMP6s	1.0/1.0	1
MA1	Isoflurane	1	Auditory	VSD	2.1/2.1	1
MA2	Isoflurane	1	Auditory	GCaMP6s	3.1/3.1	1
MA3	Isoflurane	1	Auditory	No	2.0/2.0	1
MB1	Isoflurane	1	Barrel	GCaMP6s	2.7/2.7	1
Total		8				10

Values are synchronized recording (Sync Rec) time/total recording time and number of local field potential (LFP) event clusters (LECs) for 8 recordings in mice. Recordings are identified (Rec IDs) by animal (M) and then numbered within each area (A, auditory; V, visual; B, barrel). GCaMP6s, green fluorescent calcium indicator; VSD, voltage-sensitive dye.

recording periods under reduced concentration of isoflurane (1.0–1.2%). The skull was fixed to a head plate to stabilize recording and facilitate imaging in simultaneous acquisition sessions. Extracellular recordings were made with 64-channel polytrodes (NeuroNexus A1x64-Poly2-6mm-23s-160-A64) with a two-column (32 channels per column) staggered format with vertical and horizontal (intercolumn distance) of 46  $\mu\text{m}$  covering 1,450  $\mu\text{m}$  of the probe. Voltage signals were acquired using a head-stage amplifier (RHD2164; Intan-Tech, Los Angeles, CA) and USB interface board (RHD2000; Intan-Tech) at a sampling rate of 25 kHz and with 16-bit resolution. Electrodes were inserted perpendicular to the surface of the cortex using a micromanipulator (MP-225; Sutter Instruments). Cortical penetration depth was tracked using micromanipulator coordinates with the tip of the electrode being inserted between 900 and 1,450  $\mu\text{m}$  ( $1,256 \pm 157 \mu\text{m}$ , mean  $\pm$  SD) below the cortical surface. Further details for these recordings can be found in Xiao et al. (2017). To exclude subcortical spikes and LFP, only the first 900  $\mu\text{m}$  of recorded tissue (amounting to 40 channels of the electrode) were considered for analysis.

**Mouse voltage-sensitive dye and wide-field imaging.** To determine the cortex-wide correlates of LFP event clusters (LECs), wide-field voltage-sensitive dye (VSD) imaging was carried out in anesthetized mice as previously described (Mohajerani et al. 2010, 2013; Vanni and Murphy 2014) during simultaneous extracellular recording of LFP and single-unit activity. Either a unilateral craniotomy (1 wild-type C57/BL6 mouse, from bregma 2.5 to 4.5 mm anterior-posterior and 0 to 6 mm lateral) or a bilateral craniotomy (2 wild-type C57/BL6 mice, from bregma 3.5 to 5.5 mm anterior-posterior and  $-4.5$  to 4.5 mm lateral) was made and the underlying dura removed. RH-1692 dye (Optical Imaging, New York, NY) dissolved in HEPES-buffered saline (1 mg/mL) was added to cortex for 60–90 min (Shoham et al. 1999). VSD imaging began  $\sim$ 30 min after washing of unbound dye with saline. VSD data (12-bit monochrome) was captured with 6.67-ms (150 Hz) temporal resolution using a charge-coupled device camera (model 1M60 Pantera; Dalsa, Waterloo, ON, Canada) and EPIX E4DB frame grabber with XCAP 3.1 software (EPIX, Buffalo Grove, IL).

**GCaMP6 mouse wide-field calcium imaging.** Wide-field calcium imaging was carried out in anesthetized transgenic GCaMP6 (Madisen et al. 2015) mice [C57BL/6J-Tg(Thy1-GCaMP6s)GP4.3DkIm/J] during simultaneous extracellular recording of LFP and single-unit activity as

previously described (Xiao et al. 2017). This mouse line expresses the green fluorescent calcium indicator GCaMP6s in layers 2/3 of the cortex, and the Thy1 promoter leads to expression predominantly in excitatory neurons (Dana et al. 2014).

Table 2 summarizes recording IDs, anesthetic methods, and recording duration for individual extracellular and VSD recording experiments in mice.

### Analysis

Most of the analyses were carried out using custom Python code developed as part of an electrophysiology and optical physiology toolkit currently in development (<https://github.com/catubc/openneuron>). Methods for computing event-triggered analysis for VSD imaging have been previously published (Xiao et al. 2017) and are also available online ([https://github.com/catubc/sta\\_maps](https://github.com/catubc/sta_maps)).

**Single-unit spike sorting.** Spike sorting of cat and mouse data was carried out primarily using SpikeSorter (Swindale and Spacek 2014, 2015) and selectively using Kilosort (Pachitariu et al. 2017) and JRClust (Jun et al. 2017). For recordings sorted using SpikeSorter, electrophysiological traces were high-pass filtered and spikes detected using a threshold of 5 times the median of the absolute voltage values of each channel divided by 0.675 (Quiroga et al. 2004) and by a dynamic multiphasic event detection method (Swindale and Spacek 2015). A summary of the sorting results is provided in Table 3, and examples of sorted spike waveforms are shown in Supplemental Fig. S1 (all supplemental material is available online at [https://github.com/catubc/lfp\\_cluster](https://github.com/catubc/lfp_cluster)).

**Clustering LFP events.** High-amplitude LFP events were detected and clustered by converting LFP recordings to a data format similar to that of a high-pass spike recording. Existing spike sorting tools were then used for event detection, alignment, feature extraction, clustering, and review. Synchronized states (see Fig. 1A) were identified using the deepest LFP channel and on the basis of a synchrony index (SI) (Saleem et al. 2010), which measures the ratio between low-frequency (L) and higher frequency (H) power. We defined the low-frequency band as 0.1–4.0 Hz and the higher frequency band as values  $>10$  Hz. Values of  $SI = [L/(L+H)] > 0.7$  were used to define the synchronous state. In cat V1 recordings, synchronized-state periods accounted for  $2.7 \pm 1.5$  h of a total recording time of

Table 3. *Single-unit sorting summary*

Species	Track Recording Duration, h	Neuron Yield per Track	Average No. of Spikes per Unit	Median Firing Rate, Hz	Neurons Firing <2 Hz, %
Cat (anesthetized)	$8.8 \pm 3.0$	$99 \pm 38$	31,807	0.31	86.00
Mouse (anesthetized)	$2.5 \pm 0.4$	$85 \pm 29$	11,974	0.26	89.00

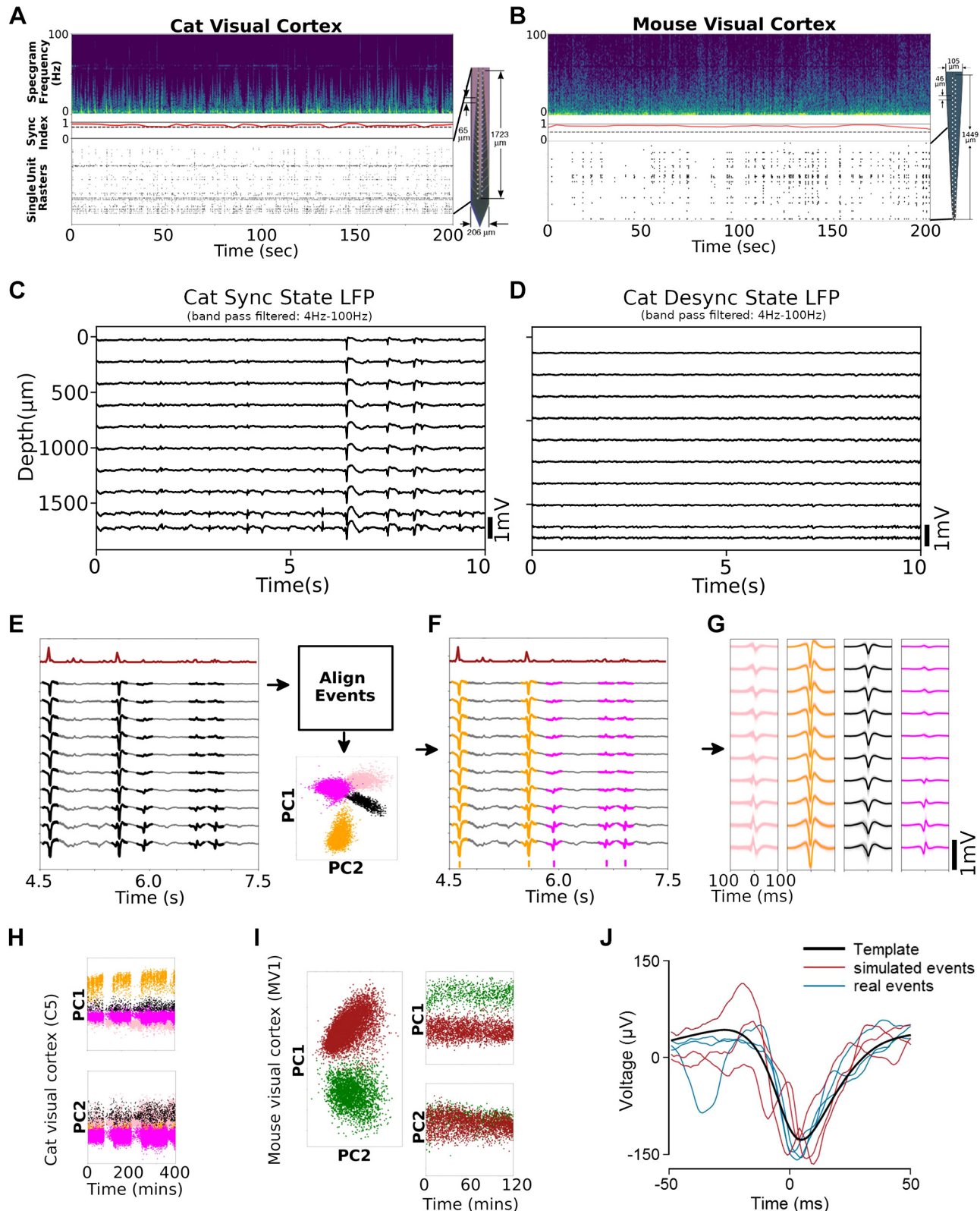
Values are means  $\pm$  SD for track recording duration and neuron yield per track.



$8.8 \pm 3.0$  h (Table 1) but varied substantially for each recording, ranging from 4% to 86% of the total recording period for each animal. This was likely due to variability of anesthetic depth and animal physiology (see Swindale and Spacek 2019). In anesthetized mouse sensory cortex recordings, synchronized-state periods

accounted for  $2.3 \pm 0.2$  h, ranging from 84% to 100% of the total recording periods (Table 2).

Synchronized-state LFP recordings were next high-pass filtered with a 4-pole Butterworth filter with a cutoff of 4 Hz to remove slower LFP fluctuations and improve signal-to-noise ratio (SNR) for subse-



quent event detection, alignment, and clustering. Next, event detection was performed using the same methods described above for spikes, with the same detection threshold and a temporal window of 50 ms (Swindale and Spacek 2015). A temporal lockout of 150 ms and a spatial lockout of 2 mm were used to ensure that in a 150-ms period, only a single LFP event could be identified. Following detection, events were initially aligned using a weighted center of gravity definition of the time of the event (Swindale and Spacek 2014). Max peak alignment revealed similar results. Principal components were then calculated on the basis of the covariance matrix obtained from the 50 points with the highest voltage variance taken across all channels. The observed principal component value distributions normally showed clear evidence of clustering (see Figs. 1E and 2). Clustering was based on the first two principal component values. Following clustering, the mean waveform of the events in the cluster was calculated, and the individual waveforms were then further aligned to this mean using root mean square (RMS) error minimization (Swindale and Spacek 2014) computed over all the LFP channels. The mean waveform was then recalculated, and the process was repeated until further realignments were of vanishingly small magnitude. The time in the aligned event waveform that corresponded to the center of gravity of the template (defined as above for individual waveforms) was then taken as the time of the event. Note that any other stable feature of the template could equally well have been used as an anchor, because this would simply change the times of all the events by the same amount. We used the center of gravity measure in preference to peaks, troughs, or zero-crossings because these features can be variable across different LECs and are occasionally ambiguous. Clusters with <20 events or with peak-to-peak heights <100  $\mu$ V were deleted and excluded from further analysis.

**Precision of estimation of event times.** The accuracy with which individual LEC events can be aligned to the template in the presence of background variability in the LFP signal determines the accuracy of the estimate of the times at which individual events can be said to have occurred. This accuracy potentially limits the ability to determine the variability in the timing of spikes of individual units relative to the event. If the accuracy is low, the measured variability in timing will be larger than it actually is. We estimated the accuracy of the RMS alignments by computing hybrid ground truth data (i.e., using real data with simulated shifts). We first calculated the mean of a number of samples (typically between 3,000 and 4,000) of individual clustered and aligned LFP event waveforms to obtain an LEC template. Each sample was 100 points long (= 100 ms) and was centered on the event as determined by RMS minimization. The mean was then subtracted from each of the samples to obtain a set of residual noise samples. The covariance matrix of these samples was calculated and factorized using Cholesky decomposition. Samples of uncorrelated Gaussian noise vectors with a standard deviation of 1 were then multiplied by the Cholesky matrix to generate noise samples with the same mean amplitude and covariance structure as the real noise. Simulated LEC waveforms were then generated by adding samples of simulated noise to the LEC template. Each waveform was then realigned to the template using RMS minimization, and the resulting

shift in position was taken as the error for that particular sample. The mean of the errors was normally close to zero, and the standard deviation of the errors measured for 1000 random samples was taken as an estimate of the accuracy.

**CSD computation.** LEC CSDs were computed by calculating the second spatial derivative (Nicholson and Freeman 1975) of LEC templates using all available LFP channels. This calculation was implemented using the gradient function of the numpy Python library, which provides “first or second order accurate one-sides (forward or backwards) differences at the boundaries” (<https://docs.scipy.org/doc/numpy-1.13.0/reference/generated/numpy.gradient.html>).

**LEC-triggered VSD motifs.** VSD motifs were computed as described by (Xiao et al. 2017). A response,  $dF/F_0$ , was computed for  $-3$  to  $+3$  s around each LEC event, with  $F_0$  calculated as the average of the signal  $-6$  to  $-3$  s before each event. Strong sensory stimulation resulted in VSD signals that generally peaked at 0.5%  $dF/F_0$ . The LEC-triggered VSD motifs had peaks of 0.1–0.2%. These were substantially larger than randomly generated motif peaks (see Fig. 6A, control).

**Grouping of LECs using CSD shapes.** CSDs from different probes were clipped to the length of the shortest probe and then clustered using a Gaussian mixture model with three components (see Fig. 2E). Because the recordings were made with electrodes of different lengths, all CSD shapes were clipped to represent only 0 to 1,200  $\mu$ m of cortical tissue. This allowed for a proper comparison to be made across all 24 selected recordings. Next, the two-dimensional (2D) CSDs were aligned to the mean of all 2D shapes by interpolating the time course fivefold and finding the best cosine similarity value. The aligned CSD were then converted to a 1D vector, and the vector array for all CSDs was compressed using principal component analysis. Last, a generalized mixture model with three components was fit to the resulting distributions (3 was chosen because qualitatively there appeared to be 3 different shapes in considering both CSD shapes and PCA distributions).

**Detection of behavioral state in rat recordings.** Behavioral state computation for the analysis of rat recordings was obtained using the Buzsáki laboratory repository and SleepScoreMaster code (<https://github.com/buzsakilab/buzcode>, accessed March 22, 2019) and the original paper (Vyazovskiy et al. 2009).

## RESULTS

### *Clustering Large-Amplitude Multilaminar LFP Events in Cat and Mouse Cortex Reveals Distinct Event Classes That Can Be Detected with Near-Millisecond Precision*

Multichannel extracellular recordings were made during synchronized states in anesthetized cat visual cortex and mouse visual, barrel, and auditory cortex (see Fig. 1A, cat visual cortex, and Fig. 1B, mouse visual cortex). Synchronized-state recordings in anesthetized cats and mice contain large-amplitude, stereotypically shaped LFP events (Fig. 1C) that were

Fig. 1. Clustering local field potential (LFP) events during synchronized cortical states. A: example of a 200-s cat visual cortex extracellular recording with power spectrogram (top), synchrony index (middle), single-neuron rasters (bottom), and 64-channel extracellular probe diagram (inset). B: same as A, but from mouse visual cortex using a different type of extracellular probe containing 64 channels. C: extracellular recording of 10 LFP channels obtained from a track in cat visual cortex during a synchronized state (bandpass filtered 1–100 Hz) reveals infrequent large-amplitude cross-laminar events (animal C5). D: same recording track as in C a few hours later shows a desynchronized cortical state lacking large-amplitude LFP events. E: large-amplitude LFP events (black bold traces) correlate with peaks in multiunit-activity (MUA) histograms (brown traces) during synchronized-state recordings (animal C5). F: large-amplitude LFP events are detected, featurized, and clustered (see text for details). G: LFP templates for the 4 LFP event clusters (LECs) identified in F show distinct multilaminar LFP patterns. H: principal component values (PC1 and PC2) for the 4 LECs shown in G, plotted over a period of 400 min (6.7 h), showing that individual LEC features are relatively stable over time. I: same as H, but for 2 LECs in a mouse visual cortex recording. J: estimating the precision of detection of LFP events using simulated and real LFP traces (see also RESULTS). Solid black line shows the average (template) of events from an example LEC. The 3 blue traces show the profiles of 3 individual events, and the 3 red traces show the profiles of simulated events obtained by adding correlated noise to the template. Event times were estimated by finding the horizontal position of a profile that minimizes the root mean square difference between it and the template. Time 0 is defined as a weighted measure of the center of gravity of the template (see MATERIALS AND METHODS). Desync, desynchronized; Specgram, spectrogram; Sync, synchronized.

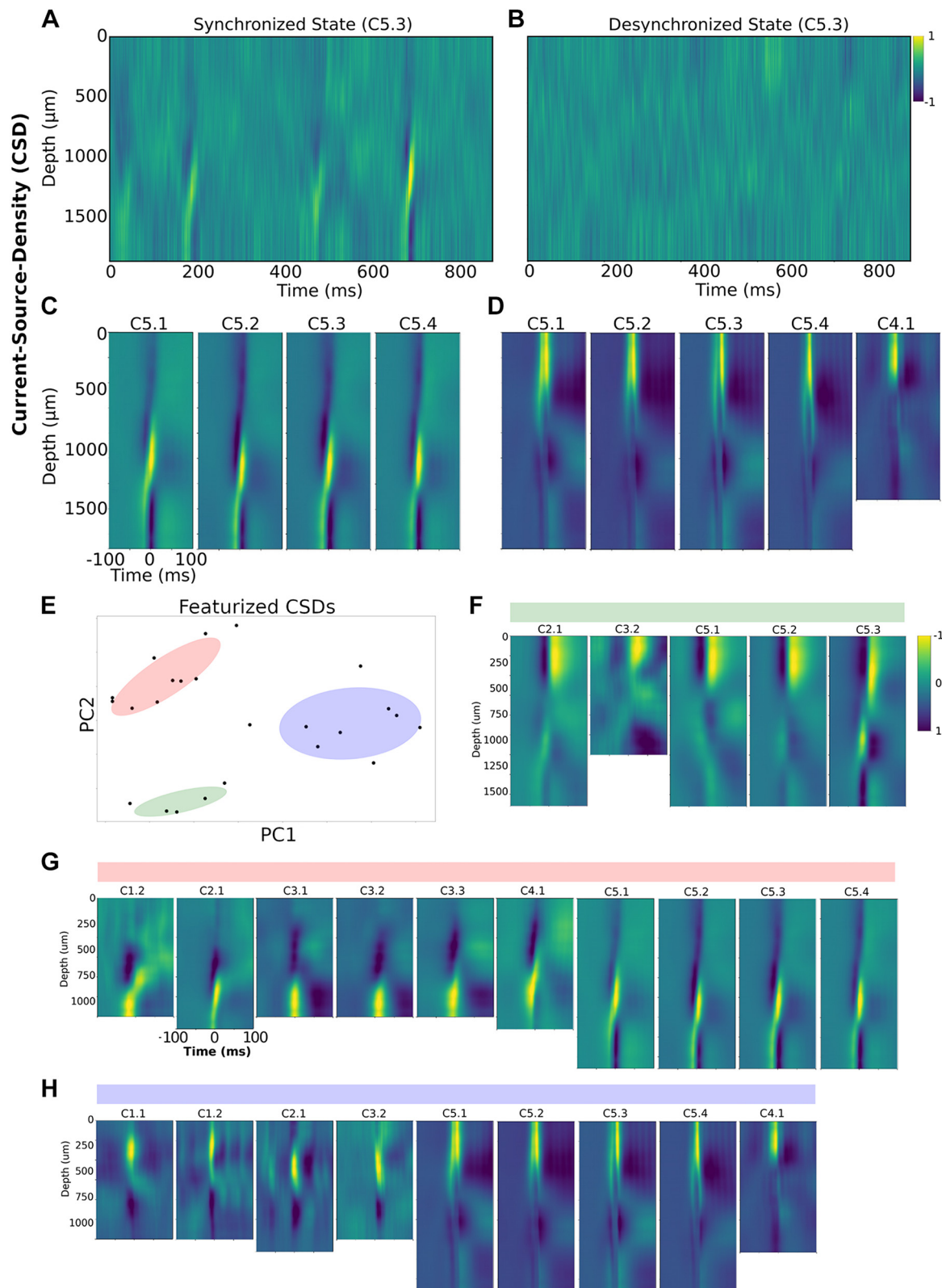


Fig. 2. Current source density (CSD) analysis of local field potential event clusters (LECs). *A*: CSD distributions for an 850-ms synchronized-state recording (same track in *animal* C5 as shown in Fig. 1*A*). *B*: CSD distributions for an 850-ms desynchronized-state recording (same track as Figs. 1*A* and 4*A*). *C*: CSD obtained from averaged LEC event profiles (i.e., templates) recorded in 4 different visual cortex tracks in *animal* C5. *D*: CSD distributions for averaged LEC profiles recorded in 5 different visual cortex tracks in 2 cats (C5.1–C5.4 and C4.1). *E*: principal component distributions for the most common 24 CSDs detected in cat visual cortex recordings were fit with a 3-component generalized Gaussian mixture model (see MATERIALS AND METHODS). Shaded regions represent 1 SD. *F–H*: CSD distributions for each group clustered in *E*.



Table 4. *Cat V1: LEC grouping summary*

Rec ID	Anesthetic	LEC Type						Other
		1	2	3	4	5	6	
C1.1	Iso/N <sub>2</sub> O		X					X
C1.2	Iso/N <sub>2</sub> O	X	X					
C2.1	Iso/N <sub>2</sub> O	X	X					
C2.2	Iso/N <sub>2</sub> O						X	
C3.1	Iso/N <sub>2</sub> O	X						
C3.2	Iso/N <sub>2</sub> O	X	X	X				
C3.3	Iso/N <sub>2</sub> O	X				X		
C3.4	Iso/N <sub>2</sub> O				X			
C4.1	Prop/Fent	X	X					
C4.2	Prop/Fent						X	X
C5.1	Prop/Fent	X	X	X				
C5.2	Prop/Fent	X	X	X				
C5.3	Prop/Fent	X	X	X				X
C5.4	Prop/Fent	X	X	X				
Total		10	9	5	1	1	2	3

Data show occurrences of local field potential event clusters (LECs) of specific types (1–6, etc.) found in specific recordings (as identified in Table 1). Totals for each column are total number of observations of each type. Recording numbers (Rec IDs) are indicated by animal (C1–C5) and then by track number in each animal. Fent, fentanyl; Iso, isoflurane; N<sub>2</sub>O, nitrous oxide; Prop, propofol.

largely absent during desynchronized cortical states, where only lower amplitude events were typically observed (Fig. 1D). Large-amplitude LFP events correlated with peaks in multiunit activity (MUA; Fig. 1E), which are commonly believed to be global indicators of Up-state transitions (Luczak et al. 2007). The LFP events generally had one to three peaks and troughs with varying relative heights and widths (Fig. 1F). Peak-to-peak amplitudes were typically 250  $\mu$ V to 1 mV (after high-pass filtering at 4 Hz), and the duration of the events was typically 50–100 ms. Polarities sometimes, but not always, reversed with depth (examples in Supplemental Fig. S2). Clustering these events (see MATERIALS AND METHODS) revealed one to four LECs per recording session in cat visual cortex and one or two LECs in mouse visual, auditory, and barrel cortex recording sessions (Fig. 1G, example cat grouping; Tables 4 and 5; see also MATERIALS AND METHODS). The overall frequency of all LECs summed together ranged from 0.5 to 2.5 Hz (in mouse, cat, and rat recordings) with individual LEC frequencies of 0.12 Hz across all cat V1 recordings (Table 6) and 0.18

Table 5. *Mouse cortex: LEC grouping summary*

Rec ID	Anesthetic	Area	LEC Type							
			1	2	3	4	5	6	7	8
MV1	Isoflurane	Visual	X	X						
MV2	Isoflurane	Visual	X							
MV3	Isoflurane	Visual	X		X	X				
MV4	Isoflurane	Visual	X			X				
MA1	Isoflurane	Auditory					X	X		
MA2	Isoflurane	Auditory						X		
MA3	Isoflurane	Auditory							X	
MB1	Isoflurane	Barrel								X
Total			4	1	1	2	1	2	1	1

Data show occurrences of local field potential event clusters (LECs) of specific types (1–8) found in specific recordings (as identified in Table 2). Totals for each column are total number of observations of each type. Recording numbers (Rec IDs) are indicated by animal (M) and then numbered within each area (A, auditory; V, visual; B, barrel).

Table 6. *Cat V1: LEC firing rates*

Rec ID	Anesthetic	LEC Type						Other
		1	2	3	4	5	6	
C1.1	Iso/N <sub>2</sub> O		0.10					0.02
C1.2	Iso/N <sub>2</sub> O	0.04	0.52					
C2.1	Iso/N <sub>2</sub> O	0.05	0.11					
C2.2	Iso/N <sub>2</sub> O						0.25	
C3.1	Iso/N <sub>2</sub> O	0.16						
C3.2	Iso/N <sub>2</sub> O	0.08	0.08	0.35				
C3.3	Iso/N <sub>2</sub> O	0.04				0.32		
C3.4	Iso/N <sub>2</sub> O				0.03			
C4.1	Prop/Fent	0.29	1.4					
C4.2	Prop/Fent						0.4	0.90
C5.1	Prop/Fent	0.31	0.04	1.74				
C5.2	Prop/Fent	0.25	1.11	0.84				
C5.3	Prop/Fent	0.32	0.24	1.68				0.09
C5.4	Prop/Fent	0.21	0.28	2.57				

Data are firing rates (Hz) of local field potential event clusters (LECs) of specific types (1–6, etc.) found in specific recordings (as identified in Table 1). Recording numbers (Rec IDs) are indicated by animal (C1–C5) and then by track number in each animal. Fent, fentanyl; Iso, isoflurane; N<sub>2</sub>O, nitrous oxide; Prop, propofol.

Hz across all mouse cortex recordings (Table 7). We provide additional examples of single LEC events clustered in mouse cortex in Supplemental Fig. S3.

We tracked the stability of the shape of each LEC event within a cluster over time using the principal component values of the LEC event waveforms. We found that LEC shapes were stable and that the principal component values of events within each cluster did not change substantially over periods of up to 3 h in either cat (Fig. 1H) or mouse (Fig. 1I) cortical recordings.

We estimated the accuracy with which the times of individual LEC events could be measured by taking individual LEC templates and adding synthetic events (containing noise of the same temporal structure as real noise; see MATERIALS AND METHODS for full details). We then measured the change in the time of the event required to minimize the RMS difference between it and the template; this change was the alignment error resulting solely from the added noise. The standard deviation of the resulting changes with repeated noise samples was taken as an estimate of the likely alignment error present with the real events in the sample. Doing this for a number of different LECs in several cat and mouse recordings revealed error estimates from 1.0 to 4.7 ms with a mean of 2.7 ms ( $n = 11$  LECs in 6 different recordings). The accuracy of the

Table 7. *Mouse cortex: LEC firing rates*

Rec ID	Anesthetic	Area	LEC Type							
			1	2	3	4	5	6	7	8
MV1	Isoflurane	Visual	0.07	0.09						
MV2	Isoflurane	Visual	0.23							
MV3	Isoflurane	Visual	0.04		0.32	0.04				
MV4	Isoflurane	Visual	0.10			0.01				
MA1	Isoflurane	Auditory					0.06	0.01		
MA2	Isoflurane	Auditory						0.09		
MA3	Isoflurane	Auditory							0.37	
MB1	Isoflurane	Barrel								0.03

Data are firing rates (Hz) of local field potential event clusters (LECs) of specific types (1–8) found in specific recordings (as identified in Table 2). Recording numbers (Rec IDs) are indicated by animal (M) and then numbered within each area (A, auditory; V, visual; B, barrel).

estimate was found to vary roughly linearly with the standard deviation of the added noise, over a range of 0–2 times the standard deviation of the original noise. Consequently, the accuracy may vary with the amplitude of the LEC template relative to the variance in the background LFP signal.

These estimates also put a lower bound on the accuracy with which spike times relative to individual LEC events can be measured. However, the estimates were based on waveform data from a single LFP channel (the largest amplitude LEC template channel). Adding additional channels improves the accuracy, although the improvements were found to be small, likely because signals tended to be highly correlated across adjacent channels. We also explored the temporal precision of LEC event detection by computing the stability of the full width at half maximum (FWHM) of the largest negative peak of each LEC event (Supplemental Fig. S4). We found that the standard deviations of the FWHM were <10 ms in most cases, further suggesting that the overall shape of the LECs is stable across time.

#### *LECs Reflect Distinct CSD Patterns Common Within and Across Animals*

We used CSD analysis (Nicholson and Freeman 1975) to further investigate the grouping of LECs within and across animals (Fig. 2; see also MATERIALS AND METHODS). As shown in the raw voltages (Fig. 1, *C* and *D*), the CSD computed from raw, unaveraged LFP traces revealed distinct patterns during synchronized states that were absent (or significantly smaller in amplitude) during desynchronized states in cat visual cortex (Fig. 2, *A* and *B*). See Supplemental Fig. S5 for a CSD profile from a mouse visual cortex recording. Computing CSD profiles for different LEC templates from several cat V1 recordings (i.e., same cat but different electrode track) showed distinct current-sink distributions with some active sources in deeper (Fig. 2*C*) or more superficial layers (Fig. 2*D*). Qualitative comparisons across different tracks within the same animal or across two animals showed that the CSDs could be nearly identical in shape and depth profile (e.g., Fig. 2*C* shows similarly shaped LEC CSD profiles from 4 different tracks in 2 hemispheres from a single cat).

We next featurized the 2-D (time vs. depth) CSD profiles for all recorded LECs in cat visual cortex and excluded outliers (Fig. 3*D*; see also MATERIALS AND METHODS). The remaining 24 LECs were fit with a Gaussian mixture model with three components, which showed that the CSDs fell into three groups. These groupings agreed with qualitative observations of similarity within each cluster, but alternative choices might be possible. We also explored t-distributed stochastic neighbor embedding (t-SNE) as a dimension reduction method, but the resulting distributions lacked obvious groupings.

Thus, rather than being unique or specific to a particular animal or track, or to a particular time segment, LECs can be grouped on the basis of their CSD shape and can have the same shape within or across different cats. This suggests that LECs may be generated by cortical circuits common within a species. Such circuits could underlie Up-state transitions.

Additionally, in a total of eight mouse recordings from visual, auditory, and barrel cortex, we found 13 LECs that could be grouped into one or two distinct classes (Table 5). We also note that we failed to observe clear peaks in the autocor-

relogram or cross-correlograms of individual events within the LECs.

#### *LECs Are Present in Naturally Sleeping Rats*

We additionally investigated LECs from extracellular recordings in chronically implanted rats in periods of non-REM natural sleep (see Fig. 3 for an example from 1 rat). We found that during non-REM periods (Fig. 3*A*), LFP recordings from multiple shanks contained large-amplitude LFP events that corresponded to single-neuron firing and peaks in MUA histograms (Fig. 3*B*). Computing CSDs from the LFP recordings (Fig. 2; see also MATERIALS AND METHODS) revealed that stereotyped LFP events could be observed on each shank (Fig. 3*C*).

Clustering the raw multichannel LFP signal as in cat and mouse recordings (Fig. 1; see also MATERIALS AND METHODS) revealed that within each shank, there were between one and two discrete clusters that contained qualitatively distinct shapes (Fig. 3, *D–F*, *top*). The LECs had distinct multichannel LFP shapes as well as CSD profiles (Fig. 3, *D–F*, *bottom*). Finally, the LEC event rate was 1.8 Hz (for each shank), and in an additional rat recording (BWRat19-032413), the rate was 1.2 Hz. These findings further extend the results from anesthetized cat and mouse recordings to naturally sleeping rats and further support LECs as being ubiquitous in multiple mammals.

#### *Most Single Neurons Fire Precisely in Relation to LECs*

We next analyzed the temporal relationship between single-unit spiking and LEC events. We first computed peri-LEC event time histograms (PLETHs) for all recorded neurons using 5-ms bins and triggering off the LEC event times (Fig. 4; see also MATERIALS AND METHODS). We found that neurons could have PLETH distributions with peaks shifted in time relative to each other (see colored traces in Fig. 4*A*, cat visual cortex recording, and Fig. 4*B*, mouse visual cortex recording). Interestingly, some neurons responded preferentially to some LECs versus others (for example, in Fig. 4*A*, blue and red neurons prefer LECs 2 and 4, respectively). This suggests that some neurons can preferentially lock to some LECs but not others (although we did not observe or evaluate this phenomenon for all recordings). The PLETH widths (FWHM) for the highest amplitude LECs within a recording (i.e., those associated with the highest net firing rates) were on the order of several milliseconds to ~50 ms, the lower values of which are an order of magnitude smaller than previously reported (e.g., Luczak et al. 2007).

Given that the PLETH peaks were often only a few milliseconds apart, we also computed a two-sample Kolmogorov–Smirnov test (KS test) to assess whether the spike distributions, not just the peaks, were different between pairs of neurons. We found that despite sparse firing for many neurons, spiking distributions were almost always different between pairs of units recorded simultaneously (i.e., more than 90% of neuron pairs had *P* values <0.01; KS tests, Bonferroni corrected; Supplemental Fig. S6). In other words, almost all neurons had unique firing distributions relative to all other neurons even though their spiking distributions fell within a window of ~25–50 ms.

Plotting the PLETHs for each neuron in a single recording and arranging neurons by peak time of firing revealed a gradual temporal difference in peaks across almost all units recorded



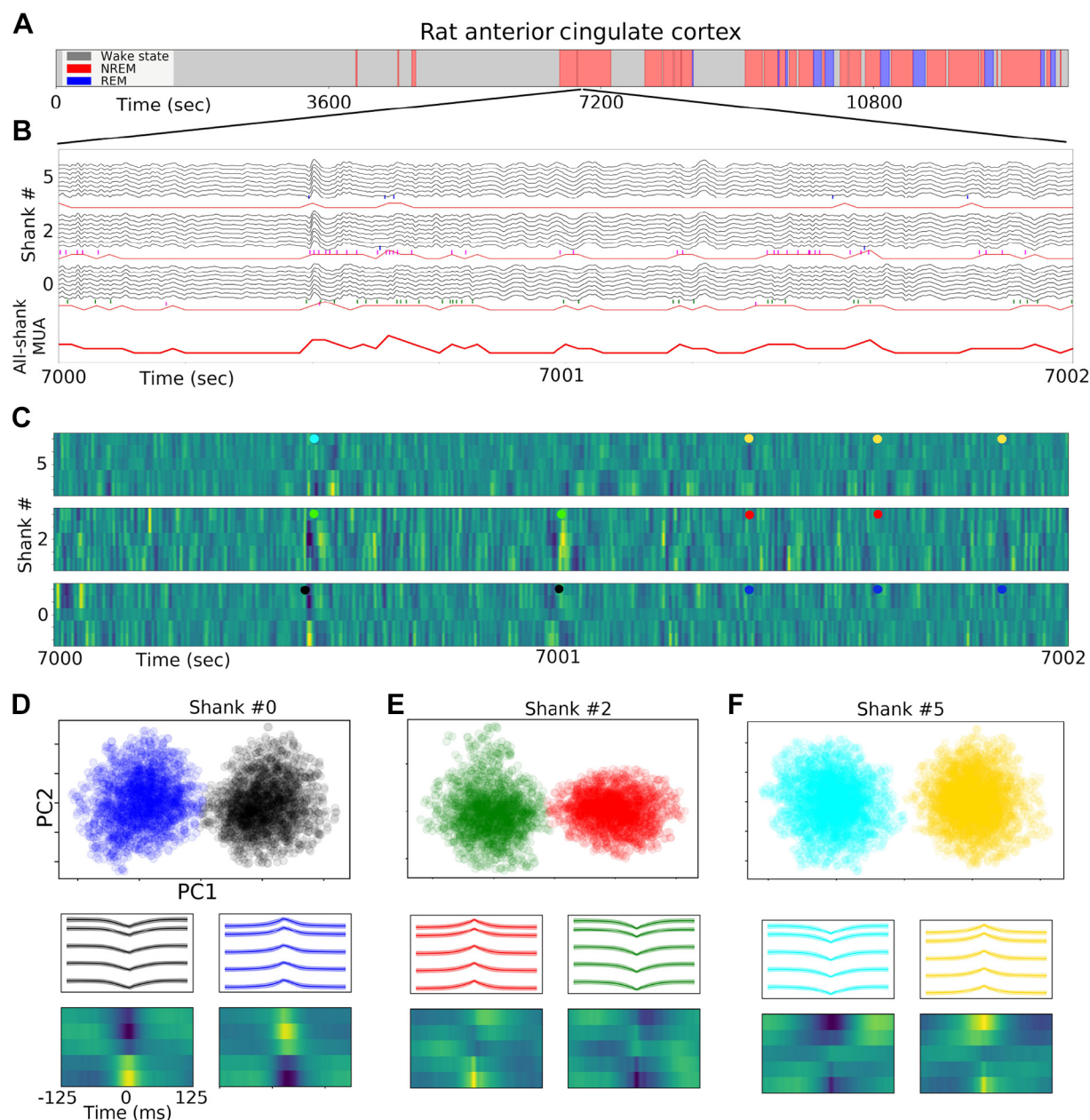


Fig. 3. Local field potential (LFP) event clusters (LECs) are present in naturally sleeping rats. *A*: brain-state timeline from an extracellular recording in rat containing wake, non-rapid-eye-movement (NREM) and rapid-eye-movement (REM) periods (see MATERIALS AND METHODS). *B*: expanded 10-s period from 4 selected shanks shows large-amplitude LFP events propagating across multiple shanks (black traces) that correlate with single-neuron spiking (colored rasters). Red traces represent multiunit-activity (MUA) histograms on each shank (lighter, thinner red traces) and across all shanks (dark red trace at bottom). *C*: CSD profiles for a 400-s period reveal that each shank has stereotyped LFP events (these are the largest amplitude events; there are many more lower signal-to-noise ratio events captured by the clustering procedure). *D*: principal components (PC1 and PC2) for clustered LFP events from shank 0 of the recording (top), LFP templates computed from the clustered LFP events (middle), and CSD profiles for the 3 LECs (bottom). *E* and *F*: same as *D*, but for shanks 2 and 5, respectively.

(Fig. 4, *C–E*, left). This revealed changes in spiking peak latency that, when the difference between the earliest and latest firing peaks was taken, could be as much as 25 ms in cats and rats (Fig. 4, *C* and *E*) or 100 ms in mice (Fig. 4*D*).

Ordering units by depth (Fig. 4, *C* and *D*, right) revealed only a small qualitative preference for deeper units to fire earlier in the recording, as reported by others (Beltramo et al. 2013; Chauvette et al. 2010; Sanchez-Vives and McCormick 2000; Volgushev et al. 2006). To quantify the preference, we divided units in the recordings into upper and lower halves

(0–425 and 425–850  $\mu\text{m}$ , respectively, for mouse recordings and 0–750 and 750–1,500  $\mu\text{m}$ , respectively, for cat recordings). We then averaged mean latencies for the upper half of neurons vs. mean latencies for the bottom half of neurons. We found that deeper neurons indeed tended to fire earlier (10 of 14 mouse recordings and 21 of 32 cat recordings; see Supplemental Fig. S7). These differences were not significant when tested separately ( $P = 0.09$  and  $0.06$ , respectively, binomial test) but were significant when both data sets were combined ( $P = 0.013$ , binomial test). In cat visual cortex recordings, we

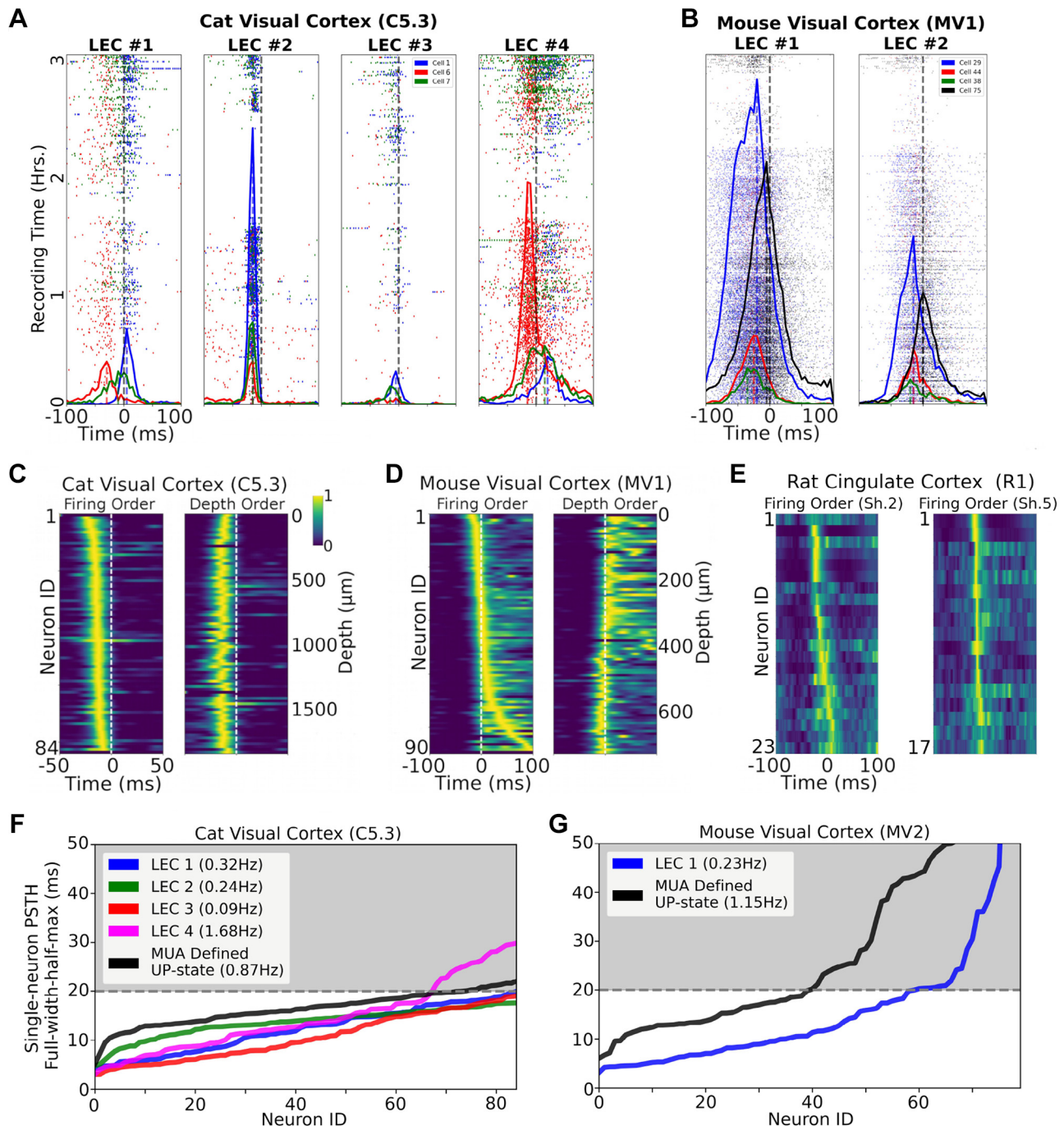


Fig. 4. Local field potential (LFP) event clusters (LECs) correlate with single-neuron activity. *A*: peri-LEC event time histograms (PLETHs) for 3 example neurons (*cells 1, 6, and 7*) and 4 LECs from a cat visual cortex recording (*C5.3*; obtained as described in MATERIALS AND METHODS). Each dot represents a spike for a particular neuron (color) relative to the LEC event time ( $t = 0$  ms; note LEC event time does not indicate the initiation of an Up state, but rather the relative center-of-gravity location in the LFP waveform, usually halfway through the LFP event). *B*: same as *A*, but from a recording in mouse visual cortex (*MV1*). *C*: PLETHs for all neurons in *A* (*LEC 2*) ordered by latency of the peak of each histogram relative to the time ( $t = 0$ ) of each LEC event (*left*; shortest latencies at *top*) or by the depth of recorded neuron (*right*). *D*: same as *C*, but from mouse visual cortex recording *MV1*. *E*: same as *C* and *D*, but from 2 different shanks in a single rat recording (*R1*; from 32 total neurons). *F*: full width at half maximum (full-width-half-max) of LEC triggered on Up-state histograms (for same neurons as in *C*) reveals that using LECs as trigger points (colored traces) yields substantially narrower distributions than multiunit activity (MUA)-defined Up states (black trace; shaded regions indicate areas where full-width-half-max measures  $>20$  ms and is a less accurate measure of single-neuron response to Up states). *G*: same as *F*, but for mouse visual cortex recording *MV2* (MUA-defined Up states used a binwidth of 10 ms and a peak threshold that provided the nearest possible firing rate to 1 Hz; see MATERIALS AND METHODS).

also found that some LECs recruited preferentially either superficial or deeper neurons (Supplemental Fig. S8).

In addition to revealing clusters of LFP events, we found that LFP event clustering provides more precise (i.e., nar-

rower) spiking distributions around LECs (Fig. 4, *F* and *G*). For example, in a cat visual cortex recording (Fig. 4*F*), we found that three of four LECs defined by LFP-based clustering yielded PLETH FWHM distributions that were sub-

stantially narrower than that defined by peaks in MUA histograms (and the 4th LEC also was more precise for most of the neurons; see Fig. 4 legend). An additional example from mouse visual cortex revealed the same (Fig. 4G).

#### Most Neurons Lock to LEC-Defined Up States with 5- to 15-ms Latencies

To quantify the temporal precision with which different units could fire in relation to the LEC, we fit PLETHs for all units using Gaussians (see MATERIALS AND METHODS). We sought to thus quantify the FWHM distributions for all units and LEC pairs across all cat and mouse recordings. We excluded unit–PLETH pairs where the standard deviation of the fitted Gaussian was  $>50$  ms (i.e., a poor fit) and where there were fewer than five spikes in the fit window (i.e., too few spikes), which resulted in exclusion of  $\sim 25\%$  of recorded units; see also MATERIALS AND METHODS). We found that many neurons had Gaussian fits with standard deviations of just a few milliseconds for both mouse (e.g., Fig. 5A) and cat cortex (Fig. 5B). Plotting the distribution of fits for all units recorded in different tracks and animals yielded an estimate of how precise the firing of a unit was relative to the LEC (Fig. 5C). Across all unit–LEC pairs measured ( $n = 3,009$ ), the mean precision

was  $\pm 11.9$  ms, although many units had lower values, with the lowest being 1.4 ms (from recording C5.3). This is close to the limit of the accuracy with which LEC event times could be measured.

#### LECs Have Broad Mesoscale Correlates in VSD Imaging of Mouse Dorsal Cortex

We additionally sought to capture the mesoscale correlates of LECs by simultaneously recording wide-field VSD signals in mouse visual and auditory cortex (Fig. 6A) and in GcaMP6 mice while recording extracellular potentials in visual, barrel, and auditory cortex (Fig. 6B). LEC-triggered averages of wide-field activity were computed as previously described (Xiao et al. 2017) for periods of  $\pm 2$  s relative to each LEC event. In VSD recordings, the spatiotemporal patterns (termed “motifs”) showed a peak at the electrode recording site and revealed gradual multiarea cortical activation preceding LEC events (Fig. 6A,  $t = 0$  s). This indicates that LECs are preceded by gradual membrane depolarizations (and potentially spiking activity) of many neurons since VSD activity represents both subthreshold and suprathreshold neural activity. This suggests that clustered LFP events are consistent with Up-state transition dynamics observed in intracellular

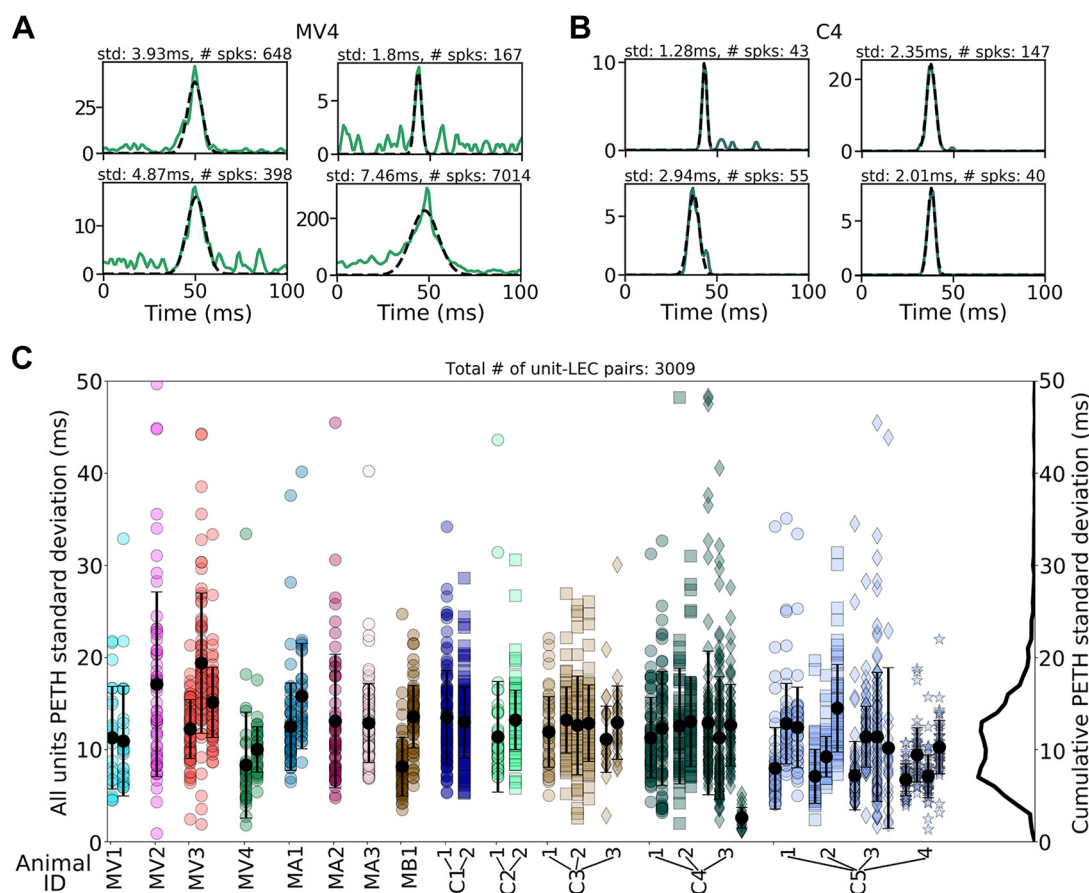


Fig. 5. Single units fire precisely in relation to local field potential event cluster (LEC) onset. *A*: peri-LEC event histograms (PLETHs; green lines) from a mouse visual cortex recording (MV4) were fit with a Gaussian function (dashed black lines) to determine the mean latency and the width of the distribution. Fits were confined to units that fired reliably in relation to the events (see RESULTS for details). *B*: same as *A*, but for a cat visual cortex recording (C4). *C*: all Gaussian fits (3,009) for each unit–LEC pair in every track for all animal recordings. Vertical axis shows the width ( $\sigma$ ) of the fitted peak for each of the selected units. Each vertical column of points (circles) is the data from a single LEC type. Columns are grouped (horizontal axis) by animal and then by track number in each animal. The narrowest widths (indicating the most precisely firing units) are  $<10$  ms. The mean and mode of the overall distribution were 11.9 and 11.0 ms, respectively. spks, spikes; std, standard deviation.



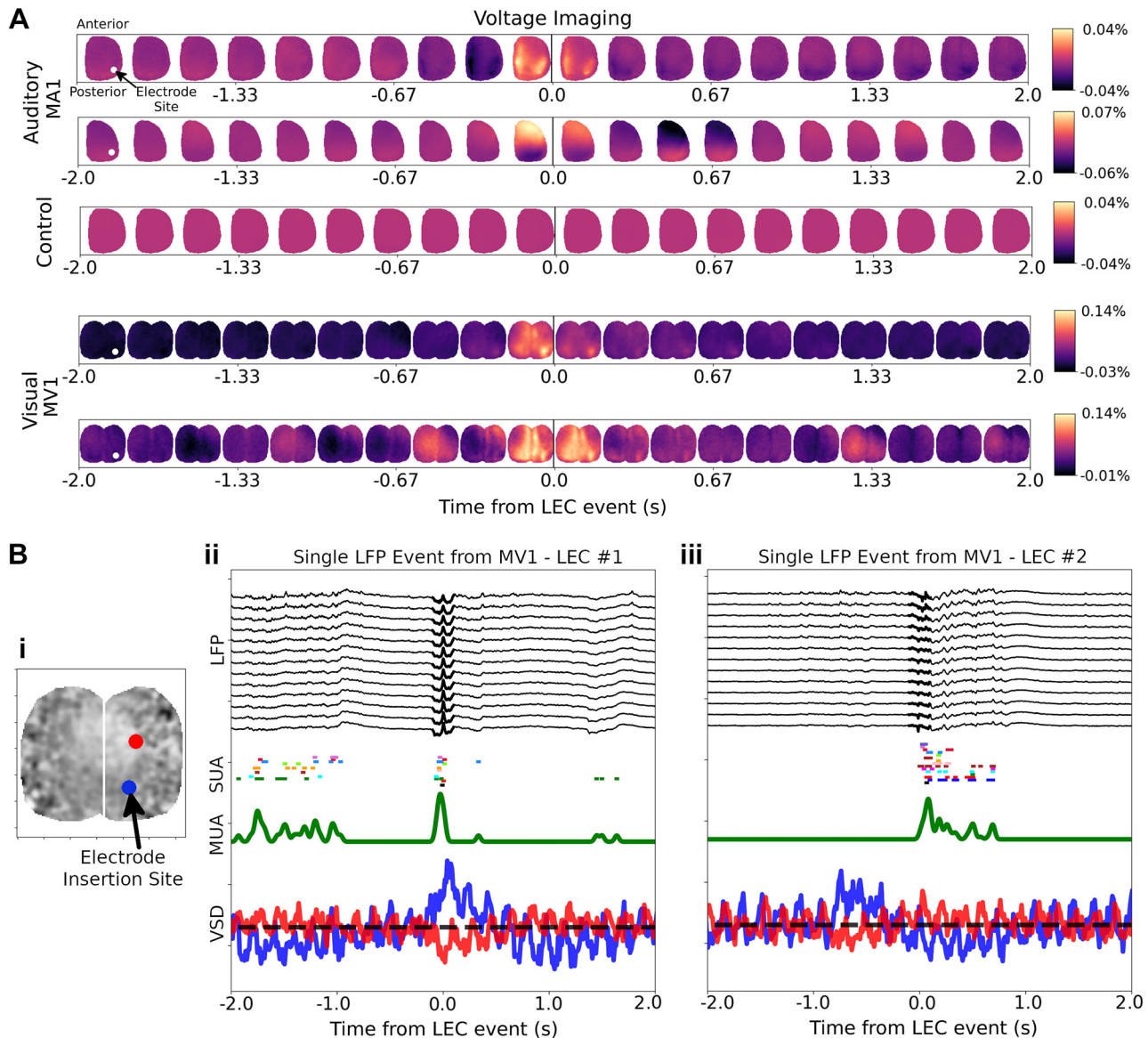


Fig. 6. Local field potential (LFP) event cluster (LEC)-triggered single- and bihemispheric wide-field voltage-sensitive dye (VSD) motifs. *A, top*: VSD imaging of LEC-triggered dynamics in an auditory cortex recording (MAI) reveals dynamics surrounding LEC event time for 2 different LECs. The control panel shows imaging data from randomly generated trigger times (controls for other experiments were similar). *Bottom*, same as *top*, but from a recording in mouse visual cortex (MVI). *B*: examples of single LEC events: *i*, location of electrode site (blue) and an additional region of interest in right hemisphere (red); *ii* and *iii*, LFP activity (black traces; high-pass filtered 4 Hz) surrounding an LEC event ( $t = 0$  s) overlaid with single-unit activity (SUA) rasters (colored scatter plots), multiunit-activity (MUA) histogram (green trace; 25-ms binwidth), and VSD activity at 2 different locations (shown in *i*).

recordings where near-simultaneous (10–100 ms) activation of neurons is observed during Up-state transitions across many cortical areas (Amzica and Steriade 1995; Destexhe et al. 1999). The findings also suggest that LECs are the LFP correlates of Up-state transitions in cortex. When considering the relationships between single LEC events and VSD imaging (Fig. 6*B*), we found that substantial spatiotemporal oscillations were present both at the electrode insertion site and in ipsilateral frontal cortex, with evidence for a peak in VSD activity at the insertion site in some cases (Fig. 6*Bii*) but not others (Fig. 6*Biii*). This suggests that whereas cortical waves could be involved in the generation of LECs, oscillations are present during most recording periods, including during nonspiking periods (i.e., between Up-state transitions).

#### LECs Have Broad Mesoscale Correlates in Calcium Imaging of Mouse Dorsal Cortex

We also carried out wide-field imaging in GCaMP6 mice while recording extracellular potentials in visual, barrel, and auditory cortex (Fig. 7). Calcium recordings revealed a somewhat different dynamic during LEC events, with largely quiescent activity preceding the onset of LEC events in mouse visual and barrel cortex (Fig. 7*A, middle* and *bottom*, respectively), but with the presence of some oscillations in auditory cortex (Fig. 7*A, top*). Single LEC event analysis further confirmed that in mouse barrel cortex (Fig. 7*B*), LEC onset coincides with strong calcium activation in barrel cortex (region contralateral to insertion site was chosen as having higher activity; see MATERIALS AND METHODS), whereas in auditory cortex, the calcium activity contained oscillations.

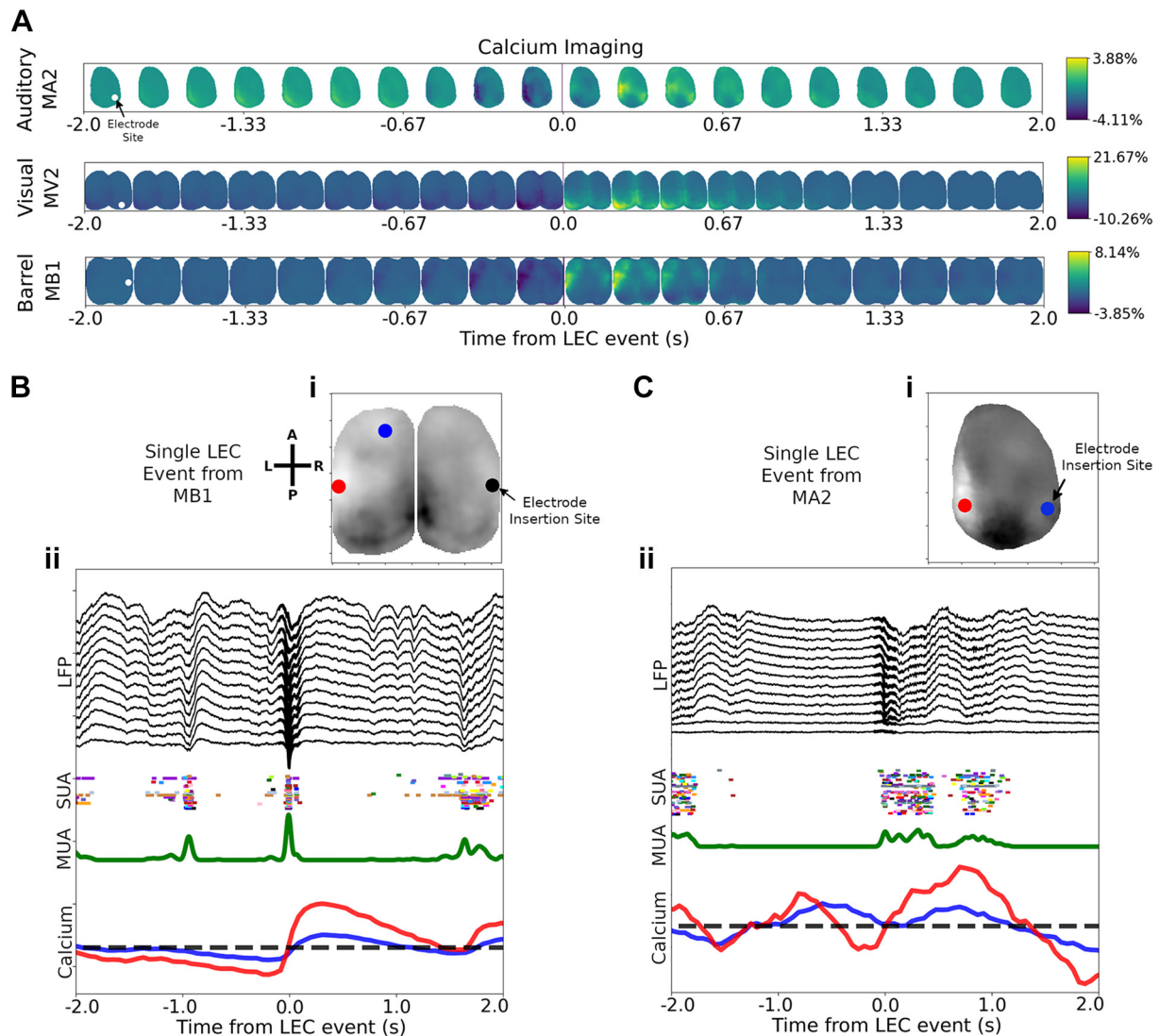


Fig. 7. Local field potential (LFP) event cluster (LEC)-triggered single- and bihemispheric wide-field calcium activity motifs. *A*: calcium imaging of LEC-triggered dynamics for wide-field recordings in mice expressing the green fluorescent calcium indicator GCaMP6s: auditory cortex recording (MA2; *top*), visual cortex recording (MV2; *middle*), and barrel cortex recording (MB1; *bottom*). *B*: single LEC event results from mouse visual cortex recording MB1 (*i*) comparing LFP, multiunit activity (MUA), single-unit activity (SUA) and calcium dynamics at specified sites (*ii*). *C*: same as *B*, but for mouse auditory cortex recording MA2 (right hemisphere). A, anterior; L, left hemisphere; P, posterior; R, right hemisphere.

## DISCUSSION

### Multiple LEC Types Suggest Multiple Sources of Up-State Genesis

It has previously been shown that Up-state transitions in single neurons have LFP correlates (Chauvette et al. 2010; Saleem et al. 2010), with recent studies using peaks in MUA as transition markers (Luczak et al. 2007, 2009; Saleem et al. 2010). In the current work we have shown that Up-state transitions can be grouped on the basis of stereotyped multi-channel LFP event shapes, revealing multiple classes of such events. We also show that most single neurons synchronize their firing to within ~25 ms of such events. The finding of multiple classes (1 to 4) of LECs in different species and cortical areas is consistent with previous work identifying stereotypy in LFP recordings (Ramirez-Villegas et al. 2015; Reichinnek et al. 2010). Another study that used MUA to define Up-state transitions found two types of transitions in

ketamine–xylazine-anesthetized rats on the basis of Up-state duration (Luczak and Barthó 2012). The findings of multiple classes of Up-state transition are also supported by CSD correlates, which have clearly different laminar patterns common across cortical areas and individuals of the same species. These findings of different patterns potentially occurring during Up-state transitions lend some support to the three-cardinal-oscillator hypothesis that Up states can be caused and sustained by potentially independent cortico-thalamo-cortical populations (Crunelli and Hughes 2010).

### Multichannel LECs Capture Global Up-State Transitions

The term “Up state” has commonly referred to a single neuron’s resting membrane potential transitioning from a hyperpolarized (i.e., nonspiking, e.g., −80 mV) to a depolarized (e.g., −60 mV) state (Wilson and Kawaguchi 1996). The term Up state also has been used to refer to a global correlate of

single-neuron Up-state transitions where many (or possibly all) cortical neurons in a region depolarize and spike simultaneously (Neske 2016). Defining an exact Up-state transition time poses certain problems. Although most (or all) neurons depolarize simultaneously during an Up-state transition, not all neurons spike on every Up-state cycle (Chauvette et al. 2010; Volgushev et al. 2006). Additionally, individual neurons depolarize at different times and rates, as indicated by measurements of their intracellular membrane potentials (Lampl et al. 1999; Petersen et al. 2003), and can have different Up-state dynamics (Ros et al. 2009).

These factors make it challenging to track Up states globally solely by recording a few neurons intracellularly or by tracking peaks in MUA. In the present study we have shown that stereotypy in the LFP waveform can be used to establish the time of each event with a precision of a few milliseconds. This marker can then serve as a physiologically relevant temporal reference for evaluating single-unit spike timing. Previous methods of identifying the time of Up-state transitions used a definition based on changes in the firing rate of simultaneously recorded neurons (Luczak et al. 2007, 2009, 2013), but these methods have the limitation that they can only be applied to high-firing-rate neurons in cortical areas that are not sparsely firing. Combined intracellular and LFP recordings (Chauvette et al. 2010; Mukowski et al. 2006) have been used to define Up-state transitions by fitting a sigmoid to LFP traces and defining a transition point at 10% of the amplitude of the sigmoid. The limitation is that both intracellular and extracellular recordings are required and that a somewhat arbitrary point is chosen as the time of the Up-state transition. Another method (Saleem et al. 2010) relies on the phase of the LFP at frequencies below 4 Hz combined with MUA and single-neuron recordings. This also has the limitation that both LFP and MUA are needed to define the onset of Up states. Overall, none of the previous work has demonstrated a particular degree of precision in defining the time of Up-state onset.

Though we claim to have found temporally precise markers of Up-state transitions, our LEC times reflect a choice in event feature location (e.g., LEC  $t = 0$  ms can be chosen at peak, trough, or center of gravity of LEC event). However, this limitation is also present in defining a global Up-state transition time using intracellular membrane potentials given that individual neurons can transition to Up states at different times (Lampl et al. 1999; Petersen et al. 2003).

### *Relation Between LECs and K-Complexes*

Like the LECs studied here, K-complexes are transient, large-amplitude events that occur in EEG or LFP recordings during the synchronized state in anesthesia and during stage 2 slow-wave sleep (e.g., Loomis et al. 1937; Amzica and Steriade 1998). In humans, K-complexes typically last up to 1 s and occur every 1–2 min. They are often followed by sleep spindles, a burst of rapid oscillations at a frequency of 11–15 Hz (De Gennaro and Ferrara 2003). In recordings from ketamine-anesthetized rats, Luczak and Barthó (2012) also describe large-amplitude fluctuations in LFP recordings that mark transitions to Up states where large numbers of neurons start firing at about the same time. That study suggests that these fluctuations are homologous to K-complexes. However, there are differences between all three sets of observations: classical

sleep-related K-complexes in humans, those of Luczak and Barthó (2012), and ours. Like those of Luczak and Barthó, our LFP “events” differ from classical K-complexes in being much faster (lasting 100–200 ms compared with up to 1 s) and occurring every few seconds (Tables 6 and 7) compared with every 1–2 min. Our events also differ from those observed by Luczak and Barthó in being simpler in structure, with typically a single large peak (positive or negative) flanked by two of opposite sign (Fig. 1G). We did not search for the traveling wave events described by Luczak and Barthó, but in future work such waves could be sought using additional data sets. We also did not observe obvious sleep spindles following our events. Reasons for these various differences would include species (human K-complexes and spindles may be generally slower than in rats and cats), the fact that the animals were not naturally sleeping, types of anesthesia (Luczak and Barthó used ketamine, whereas we used either isoflurane or propofol), and cortical area (we studied visual areas, whereas Luczak and Barthó studied rat auditory cortex). A conservative hypothesis that might reconcile all of these findings is that K-complexes constitute a large and heterogeneous class of high-amplitude transient activity in the LFP associated with Up-state transitions and widespread firing of neurons. Our findings of multiple types of LECs support such heterogeneity within single cortical areas and recording sessions, as well as suggesting that specific types of events may be identifiable within areas and across different individuals of the same species (Fig. 4).

### *LECs as Temporally Precise Global Markers of Up-State Transitions*

As an alternative global definition of Up-state transitions, LECs have advantages over single-neuron patch-clamp recordings in that they can be more rigorously defined using statistical clustering methods while also being more stable because they consist of spatially broad (i.e., 100–1,000  $\mu\text{m}$ ) LFP contributions from multiple sources (Buzsáki et al. 2012) while being largely independent of any single neuron’s activity. Although simultaneous intracellular recordings from many neurons might eventually be feasible, defining global Up-state transitions using such recordings still requires averaging Up-state transition times, leading to a definition that will be dependent on the particular set of recorded neurons. Because the LFP represents the activity of a large population of neurons, transition times estimated from the stereotyped shapes of multichannel LFP signals may provide a principled and non-circular methodology; i.e., it does not define Up-state transition spiking on the basis of cumulative spiking of many neurons.

We propose that future work should focus on the implications of the temporally precise spiking relative to Up-state transitions. This can be as low as  $\pm 1.4$  ms and, on average, was  $\pm 10$  ms. Such narrow temporal distributions lend support to the idea that spike timing and temporal order play a functional role in cortical processing (Gautrais and Thorpe 1998; Luczak et al. 2015; Panzeri et al. 2001).

### ACKNOWLEDGMENTS

We thank Pumin Wang and Cindy Jiang for surgical assistance and Jamie Boyd for technical assistance.



## GRANTS

This work was supported by Canadian Institutes of Health Research (CIHR) Operating Grants MOP-15360 (to N. V. Swindale) and MOP-12675 (to T. H. Murphy), National Science and Engineering Research Council of Canada Grant 178702 (to N. V. Swindale), and CIHR Foundation Grant FDN-143209 (to T. H. Murphy).

## DISCLOSURES

No conflicts of interest, financial or otherwise, are declared by the authors.

## AUTHOR CONTRIBUTIONS

C.C.M., M.A.S., A.W.C., T.H.M., and N.V.S. conceived and designed research; C.C.M., M.A.S., A.W.C., and N.V.S. performed experiments; C.C.M. and N.V.S. analyzed data; C.C.M. and N.V.S. interpreted results of experiments; C.C.M. and N.V.S. prepared figures; C.C.M. drafted manuscript; C.C.M., M.A.S., A.W.C., T.H.M., and N.V.S. edited and revised manuscript; C.C.M., M.A.S., A.W.C., T.H.M., and N.V.S. approved final version of manuscript.

## REFERENCES

- Amzica F, Steriade M. Short- and long-range neuronal synchronization of the slow (<1 Hz) cortical oscillation. *J Neurophysiol* 73: 20–38, 1995. doi:10.1152/jn.1995.73.1.20.
- Amzica F, Steriade M. Electrophysiological correlates of sleep delta waves. *Electroencephalogr Clin Neurophysiol* 107: 69–83, 1998. doi:10.1016/S0013-4694(98)00051-0.
- Beltramo R, D'Urso G, Dal Maschio M, Farisello P, Bovetti S, Clovis Y, Lassi G, Tucci V, De Pietri Tonelli D, Fellin T. Layer-specific excitatory circuits differentially control recurrent network dynamics in the neocortex. *Nat Neurosci* 16: 227–234, 2013. doi:10.1038/nn.3306.
- Bermudez Contreras EJ, Schjetnan AG, Muhammad A, Bartho P, McNaughton BL, Kolb B, Gruber AJ, Luczak A. Formation and reverberation of sequential neural activity patterns evoked by sensory stimulation are enhanced during cortical desynchronization. *Neuron* 79: 555–566, 2013. doi:10.1016/j.neuron.2013.06.013.
- Blanche TJ, Spacek MA, Hetke JF, Swindale NV. Polytrodes: high-density silicon electrode arrays for large-scale multiunit recording. *J Neurophysiol* 93: 2987–3000, 2005. doi:10.1152/jn.01023.2004.
- Buzsáki G, Anastassiou CA, Koch C. The origin of extracellular fields and currents—EEG, ECoG, LFP and spikes. *Nat Rev Neurosci* 13: 407–420, 2012. doi:10.1038/nrn3241.
- Chauvette S, Volgushev M, Timofeev I. Origin of active states in local neocortical networks during slow sleep oscillation. *Cereb Cortex* 20: 2660–2674, 2010. doi:10.1093/cercor/bhq009.
- Crunelli V, Hughes SW. The slow (<1 Hz) rhythm of non-REM sleep: a dialogue between three cardinal oscillators. *Nat Neurosci* 13: 9–17, 2010. doi:10.1038/nn.2445.
- Dana H, Chen TW, Hu A, Shields BC, Guo C, Looger LL, Kim DS, Svoboda K. Thy1-GCaMP6 transgenic mice for neuronal population imaging in vivo. *PLoS One* 9: e108697, 2014. doi:10.1371/journal.pone.0108697.
- De Gennaro L, Ferrara M. Sleep spindles: an overview. *Sleep Med Rev* 7: 423–440, 2003. doi:10.1053/smr.2002.0252.
- Destexhe A, Contreras D, Steriade M. Spatiotemporal analysis of local field potentials and unit discharges in cat cerebral cortex during natural wake and sleep states. *J Neurosci* 19: 4595–4608, 1999. doi:10.1523/JNEUROSCI.19-11-04595.1999.
- Gautrais J, Thorpe S. Rate coding versus temporal order coding: a theoretical approach. *Biosystems* 48: 57–65, 1998. doi:10.1016/S0303-2647(98)00050-1.
- Haider B, Duque A, Hasenstaub AR, McCormick DA. Neocortical network activity in vivo is generated through a dynamic balance of excitation and inhibition. *J Neurosci* 26: 4535–4545, 2006. doi:10.1523/JNEUROSCI.5297-05.2006.
- Harris KD, Thiele A. Cortical state and attention. *Nat Rev Neurosci* 12: 509–523, 2011. doi:10.1038/nrn3084.
- Jun J, Mitelut C, Lai C, Gratiy S, Anastassiou C, Harris T. Real-time spike sorting platform for high-density extracellular probes with ground-truth validation and drift correction (Preprint). *bioRxiv* 101030, 2017. doi:10.1101/101030.
- Lampl I, Reichova I, Ferster D. Synchronous membrane potential fluctuations in neurons of the cat visual cortex. *Neuron* 22: 361–374, 1999. doi:10.1016/S0896-6273(00)81096-X.
- Loomis A, Harvey E, Hobart G. Cerebral states during sleep, as studied by human brain potentials. *J Exp Psychol* 21: 127–144, 1937. doi:10.1037/h0057431.
- Luczak A, Barthó P. Consistent sequential activity across diverse forms of UP states under ketamine anesthesia. *Eur J Neurosci* 36: 2830–2838, 2012. doi:10.1111/j.1460-9568.2012.08201.x.
- Luczak A, Barthó P, Harris KD. Spontaneous events outline the realm of possible sensory responses in neocortical populations. *Neuron* 62: 413–425, 2009. doi:10.1016/j.neuron.2009.03.014.
- Luczak A, Bartho P, Harris KD. Gating of sensory input by spontaneous cortical activity. *J Neurosci* 33: 1684–1695, 2013. doi:10.1523/JNEUROSCI.2928-12.2013.
- Luczak A, Barthó P, Marguet SL, Buzsáki G, Harris KD. Sequential structure of neocortical spontaneous activity in vivo. *Proc Natl Acad Sci USA* 104: 347–352, 2007. doi:10.1073/pnas.0605643104.
- Luczak A, McNaughton BL, Harris KD. Packet-based communication in the cortex. *Nat Rev Neurosci* 16: 745–755, 2015. doi:10.1038/nrn4026.
- Madisen L, Garner AR, Shimaoka D, Chuong AS, Klapoetke NC, Li L, van der Bourg A, Niino Y, Egolf L, Monetti C, Gu H, Mills M, Cheng A, Tasic B, Nguyen TN, Sunkin SM, Benucci A, Nagy A, Miyawaki A, Helmchen F, Emppson RM, Knöpfel T, Boyden ES, Reid RC, Carandini M, Zeng H. Transgenic mice for intersectional targeting of neural sensors and effectors with high specificity and performance. *Neuron* 85: 942–958, 2015. doi:10.1016/j.neuron.2015.02.022.
- McCormick D, Shu Y, Hasenstaub A. *Balanced recurrent excitation and inhibition in local cortical networks*. In: *Excitatory-Inhibitory Balance: Synapses, Circuits, Systems*, edited by Hensch TK, Fagioli M. New York: Kluwer Academic/Plenum, 2004, p. 113–122.
- McCormick D, Yuste R. *Up states and cortical dynamics*. In: *Microcircuits: the Interface Between Neurons and Global Brain Function*, edited by Grillner S, Graybiel AM. Cambridge, MA: MIT Press, 2006, p. 327–346.
- Mohajerani MH, Chan AW, Mohsenvand M, LeDue J, Liu R, McVea DA, Boyd JD, Wang YT, Reimers M, Murphy TH. Spontaneous cortical activity alternates between motifs defined by regional axonal projections. *Nat Neurosci* 16: 1426–1435, 2013. doi:10.1038/nn.3499.
- Mohajerani MH, McVea DA, Fingas M, Murphy TH. Mirrored bilateral slow-wave cortical activity within local circuits revealed by fast bihemispheric voltage-sensitive dye imaging in anesthetized and awake mice. *J Neurosci* 30: 3745–3751, 2010. doi:10.1523/JNEUROSCI.6437-09.2010.
- Mukovski M, Chauvette S, Timofeev I, Volgushev M. Detection of active and silent states in neocortical neurons from the field potential signal during slow-wave sleep. *Cereb Cortex* 17: 400–414, 2006. doi:10.1093/cercor/bhj157.
- Neske GT. The slow oscillation in cortical and thalamic networks: mechanisms and functions. *Front Neural Circuits* 9: 88, 2016. doi:10.3389/fncir.2015.00088.
- Nicholson C, Freeman JA. Theory of current source-density analysis and determination of conductivity tensor for anuran cerebellum. *J Neurophysiol* 38: 356–368, 1975. doi:10.1152/jn.1975.38.2.356.
- Pachitariu M, Stringer C, Dipoppa M, Schröder S, Rossi LF, Dalgleish H, Carandini M, Harris KD. Suite2p: beyond 10,000 neurons with standard two-photon microscopy (Preprint). *bioRxiv* 061507, 2017. doi:10.1101/061507.
- Panzer S, Petersen RS, Schultz SR, Lebedev M, Diamond ME. The role of spike timing in the coding of stimulus location in rat somatosensory cortex. *Neuron* 29: 769–777, 2001. doi:10.1016/S0896-6273(01)00251-3.
- Petersen CC, Hahn TT, Mehta M, Grinvald A, Sakmann B. Interaction of sensory responses with spontaneous depolarization in layer 2/3 barrel cortex. *Proc Natl Acad Sci USA* 100: 13638–13643, 2003. doi:10.1073/pnas.2235811100.
- Quiroga RQ, Nadasdy Z, Ben-Shaul Y. Unsupervised spike detection and sorting with wavelets and superparamagnetic clustering. *Neural Comput* 16: 1661–1687, 2004. doi:10.1162/089976604774201631.
- Ramirez-Villegas JF, Logothetis NK, Besserve M. Diversity of sharp-wave-ripple LFP signatures reveals differentiated brain-wide dynamical events. *Proc Natl Acad Sci USA* 112: E6379–E6387, 2015. doi:10.1073/pnas.1518257112.
- Reichinnek S, Künsting T, Draguhn A, Both M. Field potential signature of distinct multicellular activity patterns in the mouse hippocampus. *J Neurosci* 30: 15441–15449, 2010. doi:10.1523/JNEUROSCI.2535-10.2010.

- Ros H, Sachdev RNS, Yu Y, Šestan N, McCormick DA. Neocortical networks entrain neuronal circuits in cerebellar cortex. *J Neurosci* 29: 10309–10320, 2009. doi:10.1523/JNEUROSCI.2327-09.2009.
- Saleem AB, Chadderton P, Apergis-Schoute J, Harris KD, Schultz SR. Methods for predicting cortical UP and DOWN states from the phase of deep layer local field potentials. *J Comput Neurosci* 29: 49–62, 2010. doi:10.1007/s10827-010-0228-5.
- Sanchez-Vives MV, Massimini M, Mattia M. Shaping the default activity pattern of the cortical network. *Neuron* 94: 993–1001, 2017. doi:10.1016/j.neuron.2017.05.015.
- Sanchez-Vives MV, McCormick DA. Cellular and network mechanisms of rhythmic recurrent activity in neocortex. *Nat Neurosci* 3: 1027–1034, 2000. doi:10.1038/79848.
- Seamari Y, Narváez JA, Vico FJ, Lobo D, Sanchez-Vives MV. Robust off- and online separation of intracellularly recorded up and down cortical states. *PLoS One* 2: e888, 2007. [Erratum in *PLoS One* 4: 10.1371/annotation/90ea969c-7ada-4538-aa24-17878562b995.] doi:10.1371/journal.pone.0000888.
- Shoham D, Glaser DE, Arieli A, Kenet T, Wijnbergen C, Toledo Y, Hildesheim R, Grinvald A. Imaging cortical dynamics at high spatial and temporal resolution with novel blue voltage-sensitive dyes. *Neuron* 24: 791–802, 1999. doi:10.1016/S0896-6273(00)81027-2.
- Sirota A, Buzsáki G. Interaction between neocortical and hippocampal networks via slow oscillations. *Thalamus Relat Syst* 3: 245–259, 2005. doi:10.1017/S1472928807000258.
- Sirota A, Csicsvari J, Buhl D, Buzsáki G. Communication between neocortex and hippocampus during sleep in rodents. *Proc Natl Acad Sci USA* 100: 2065–2069, 2003. doi:10.1073/pnas.0437938100.
- Steriade M. Impact of network activities on neuronal properties in corticothalamic systems. *J Neurophysiol* 86: 1–39, 2001. doi:10.1152/jn.2001.86.1.1.
- Steriade M, Nuñez A, Amzica F. A novel slow (< 1 Hz) oscillation of neocortical neurons in vivo: depolarizing and hyperpolarizing components. *J Neurosci* 13: 3252–3265, 1993. doi:10.1523/JNEUROSCI.13-08-03252.1993.
- Swindale NV, Spacek MA. Spike sorting for polytrodes: a divide and conquer approach. *Front Syst Neurosci* 8: 6, 2014. doi:10.3389/fnsys.2014.00006.
- Swindale NV, Spacek MA. Spike detection methods for polytrodes and high density microelectrode arrays. *J Comput Neurosci* 38: 249–261, 2015. doi:10.1007/s10827-014-0539-z.
- Swindale NV, Spacek MA. Visual cortex neurons phase-lock selectively to subsets of LFP oscillations. *J Neurophysiol* 121: 2364–2378, 2019. doi:10.1152/jn.00496.2018.
- Vanni MP, Murphy TH. Mesoscale transcranial spontaneous activity mapping in GCaMP3 transgenic mice reveals extensive reciprocal connections between areas of somatomotor cortex. *J Neurosci* 34: 15931–15946, 2014. doi:10.1523/JNEUROSCI.1818-14.2014.
- Volgushev M, Chauvette S, Mukovski M, Timofeev I. Precise long-range synchronization of activity and silence in neocortical neurons during slow-wave sleep. *J Neurosci* 26: 5665–5672, 2006. doi:10.1523/JNEUROSCI.0279-06.2006.
- Vyazovskiy VV, Olcese U, Lazimy YM, Faraguna U, Esser SK, Williams JC, Cirelli C, Tononi G. Cortical firing and sleep homeostasis. *Neuron* 63: 865–878, 2009. doi:10.1016/j.neuron.2009.08.024.
- Watson BO, Levenstein D, Greene JP, Gelinás JN, Buzsáki G. Network homeostasis and state dynamics of neocortical sleep. *Neuron* 90: 839–852, 2016. doi:10.1016/j.neuron.2016.03.036.
- Wilson CJ, Kawaguchi Y. The origins of two-state spontaneous membrane potential fluctuations of neostriatal spiny neurons. *J Neurosci* 16: 2397–2410, 1996. doi:10.1523/JNEUROSCI.16-07-02397.1996.
- Wilson FA, O'Scalaidhe SP, Goldman-Rakic PS. Functional synergism between putative  $\gamma$ -aminobutyrate-containing neurons and pyramidal neurons in prefrontal cortex. *Proc Natl Acad Sci USA* 91: 4009–4013, 1994. doi:10.1073/pnas.91.9.4009.
- Xiao D, Vanni MP, Mitelut CC, Chan AW, LeDue JM, Xie Y, Chen AC, Swindale NV, Murphy TH. Mapping cortical mesoscopic networks of single spiking cortical or sub-cortical neurons. *eLife* 6: e19976, 2017. doi:10.7554/eLife.19976.